# Investigation of Structural, Morphological and Optical Properties of Sulfur Doped Zinc Oxide Nanorod

Ari Sulistyo Rini[1*], Yolanda Rati[1], Akrajas Ali Umar[2] and Nur Adliha Abdullah[2]

*[1]Department of Physics, Faculty of Mathematics and Science, Universitas Riau, Kampus Bina Widya, Jl. H.R Soebrantas Km 12.5, Simpang Baru, Pekanbaru, 28293, Indonesia.*
*[2]Institute of Microengineering and Nanoelectronics (IMEN), Universiti Kebangsaan Malaysia, 43600 UKM Bangi, Selangor, Malaysia.*

## ABSTRACT

*In this study, seed-mediated hydrothermal methods has been used to fabricate sulfur-doped zinc oxide (S-ZnO) thin films with various atomic concentration of sulfur (S) (0 at.%, 1 at.%, 2.5 at.%, 5 at.% and 10 at.%). The growth process was conducted at 90 °C for 5 hours by the varying concentrations of sodium sulfide ($Na_2S$). X-Ray diffraction (XRD) analysis revealed that thin films are a hexagonal wurtzite polycrystalline structure, and the size of the crystal was slightly changed with the addition of S. The field effect scanning electron microscopy (FESEM) images showed the geometrical shape of the S-ZnO samples were nanorod with hexagonal cross section. The UV-Vis absorbance spectrum for all samples occurred in the wavelength range of 300-380 nm and 380-800 nm for high and low absorbance. The energy gap of the S-ZnO samples are in the range of 3.25-3.30 eV. The photoluminescence spectrum shows that the peak emission that occurs at a wavelength of 406 nm is the violet emission.*

**Keywords:** Zinc Oxide, Nanorod, Sulfur, Doping, Seed-Mediated Hydrothermal.

## 1. INTRODUCTION

Research on one-dimensional (1-D) nanostructured materials has become one of the interesting topics in the subject of physics, especially material science. ZnO (zinc oxide) is one of the II-VI group semiconductor materials with a wide band gap of ∼3.37 eV and an exciton binding energy of 60 meV at room temperature. ZnO possesses high optical transmittance characteristics, high electron mobility, and good chemical and mechanical stability [1]. Due to. its interesting properties, nanostructured ZnO can be applied in various fields such as gas sensors, solar cells, biosensors and piezoelectric [2].

In recent years, there have been many modifications to the properties of nanostructured ZnO by giving impurity atoms (i.e. doping). Research on doped metal oxide has been widely reported. Doping certain elements in ZnO semiconductors has a positive effect on the optical and magnetic electrical properties of the material. Some metal elements that have been successfully doped on ZnO nanoparticles including Mn [3], Al [4], Ni [5], and Mg [6]. ZnO doping by anions from chalcogen element has still limitedly reported. Sulfur (S) doping is expected to improve the physical and optical properties of nanomaterials in order to increase electron mobility [7], modify photocatalytic activity and lowering charge carrier recombination [8]. This study is still relatively rare due to the significant differences in stabilization and growth temperature of S and ZnO [9].

Various synthesis methods have successfully produced nanostructured S-doped ZnO with different morphological shape such as nanorod [8], nanotube [10], nanowire [11], and nanobelt [12][13]. The synthesis method strongly affects the morphology, particle size and physical properties of material.

---

[*]Corresponding Author: *Ari.sulistyo@lecturer.unri.ac.id*

Until now, the fabrication of nano-sized S-doped ZnO has been carried out in various ways including using the thermal evaporation [13], and Pulsed-Laser Deposition (LPD) [14]. Those kinds of methods require a special equipment at high temperature. Seed mediated hydrothermal methods offer a simple and benign procedure at low temperature. The use of this method aims to carry out 1-dimension S-doped ZnO synthesis with low temperatures and easier fabrication stages.

In this paper, sulfur doped ZnO (S-ZnO) nanorod with different S/ZnO atomic ratio of 0 at.%, 1 at.%, 2.5 at.%, 5 at.% and 10 at.% have been synthesized via seed-mediated hydrothermal under mild conditions. ZnO seed film were previously prepared by spin-coating then followed by immersing the film in the mixture of zinc nitrate hexahydrate and sodium sulfide solution. The effect of S doping concentration on ZnO nanorods were studied on the size, crystallinity, morphology, and optical properties using X-ray diffraction spectroscopy (XRD), field emission scanning electron microscopy (FESEM), energy-dispersive X-ray spectroscopy (EDX), ultraviolet–visible (UV–Vis) absorption and room temperature photoluminescence (PL).

## 2. MATERIAL AND METHODS

### 2.1 Materials

The chemicals used in this study were zinc acetate dihydrate $Zn(CH_3COO)_2.2H_2O$ ($\geq$ 99.0% ACS Reagent, Sigma Aldrich), absolute ethanol $C_2H_5OH$ (99%, HmbG® Chemicals), zinc nitrate hexahydrate $Zn(NO_3)_2.6H_2O$ (Analytical Reagent, R&M Chemicals), hexamethylenetetramine (HMT) $(CH_2)_6N_4$ ($\geq$ 99.0 % ACS Reagent, Sigma Aldrich), sodium sulfide $Na_2S$ (R & M Chemicals) and deionized water ($\sim 18\Omega$).

### 2.2. Synthesis of Pure and S-doped ZnO Nanorods

Pure and S-doped ZnO nanorod thin film were synthesized using the seed-mediated hydrothermal method which conducted in two steps, i.e ZnO seeding and S-ZnO growth. Typically, at seeding process, 10 mM zinc acetate Zn $(CH_3COO)_2.2H_2O$ in absolute ethanol was dripped onto the cleaned FTO substrate, then spin coated at 3000 rpm for 30 s and heated on a hot plate at 100 °C for 15 minutes. This process was repeated for three times in order to obtain homogeneous layer of ZnO seeds. Finally, the samples were annealed at 275 °C for 1 hour. At undoped-ZnO growth process, ZnO seed was immersed in growing solution contains zinc nitrate hexahydrate Zn $(NO_3)_2.6H_2O$ and hexamethylenetetramine $(CH_2)_6N_4$. The growing solution was dissolved in 5.0 mL deionized water with an equimolar concentration of 50 mM. For S-doped ZnO (S-ZnO) growing process, 25 uL sodium sulfide $Na_2S$ was added into the growing solution. The growing process was carried out in an electric oven at 90 °C for 5 hours. After the growth process completed, the sample was taken out from solution, then rinsed with considerable amount deionized water and dried using a flow of nitrogen gas. In this S-ZnO synthesis, 25 μL $Na_2S$ solution were added with various concentrations (10 mM, 25 mM, 50 mM, and 100 M) to obtain 1, 2.5, 5 and 10 at.% of S/ZnO, respectively.

### 2.3 Characterization

The structure, morphology and optical properties of S-doped and pure ZnO nanorods were characterized by X-ray diffraction (XRD, using a BRUKER EIXS type diffractometer), field emission scanning electron microscope (FESEM, ZEISS MERLIN type, Compact Co. Ltd.), UV-Vis spectrophotometer HITACHI U-3900H and FLS920 photoluminescence spectrometers (Edinburgh instruments) respectively.
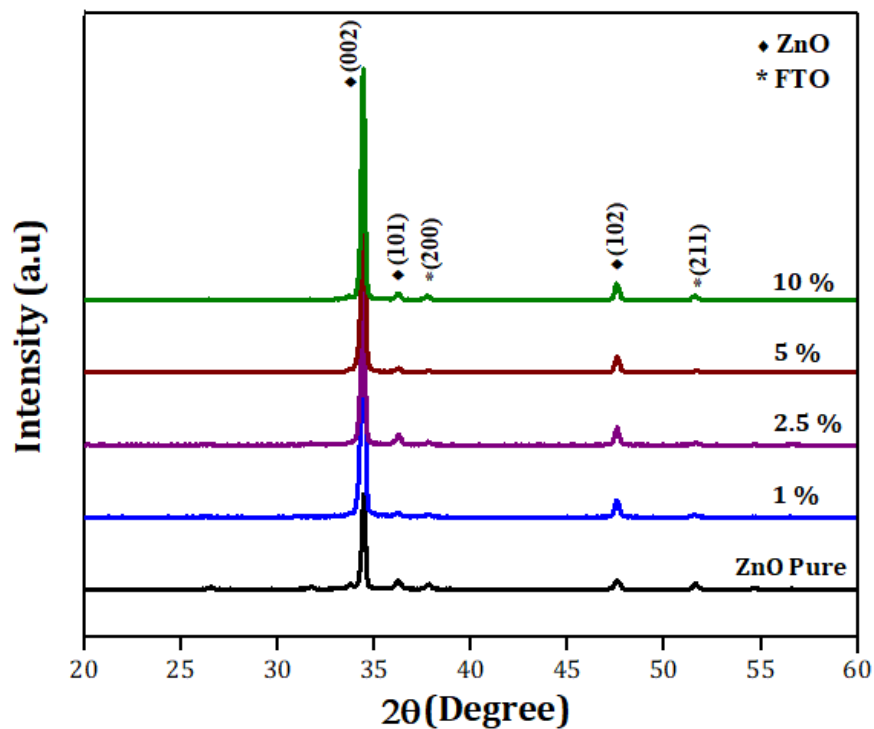
## 3. RESULTS AND DISCUSSION

### 3.1 XRD Analysis



**Figure 1.** XRD patterns of pure and S doped ZnO.

The X-ray diffraction pattern of pure and doped ZnO with different atomic ratio of S/ZnO were displayed in Fig. 1. The XRD pattern of ZnO pure shows diffraction peaks at the angle of 2θ = 34.43°; 36.26° and 47.54° which matched with the diffraction peaks of the hexagonal wurtzite crystal structure that corresponds to (002), (101), and (102) crystal plane of ZnO [JCPDS 01-075-0576]. Another diffraction peaks (*) are suggested a presence of $SnO_2$ from the FTO substrates, based on COD No. 96-210-1854. The FTO diffraction peaks are clearly seen in pure ZnO samples, and gradually decrease by the addition of sulfur that most probably due to the homogenously covering of FTO layer by S-ZnO thin film.

The XRD pattern of ZnO pure and doped ZnO shows a characteristic pattern of nanorod with growth direction of (002) [5]. The sharp and strong diffraction peaks indicate high crystallinity of the sample [9]. The XRD pattern also designates (002) as the preferred orientation of S-doped and pure ZnO. This result is in accordance with Raj [15] which shows that the orientation of the growth ZnO nanorod is in the direction of the c-axis which is perpendicular to the surface of the FTO substrate [16].

Figure 2 shows magnification of (002) diffraction peak. We can see that the (002) peak positions are slightly shifts to a smaller angle after the addition of sulfur. The diffraction peak of S-doped ZnO is shifted 0.03°, 0.04°, 0.02°, and 0.03° smaller than that of the pure ZnO (002) at 34.45° for S/Zn atomic ratio of 1 at.%, 2.5 at.%, 5 at.% and 10 at.%, respectively. This peak alteration suggested the occupation of sulfur in interstitial or oxygen site in ZnO crystal lattice [9]. By considering the larger ionic radius of $S^{2-}$ (1.80 nm) than ionic radius of $O^{2-}$ (1.40 nm), addition more sulfur will cause strain in ZnO and change the lattice parameter which leads to small diffraction angle as shown in Table 2 [9]. Relation between diffraction angle and the interplanar distance (d) is followed Bragg's law as follow,

$$n\lambda = 2d \sin \sin \theta \qquad (1)$$

where n is an integer (n = 1) and θ corresponds to the half-diffraction angle. The smaller the diffraction angle, the larger the distance $d_{200}$ of each film.
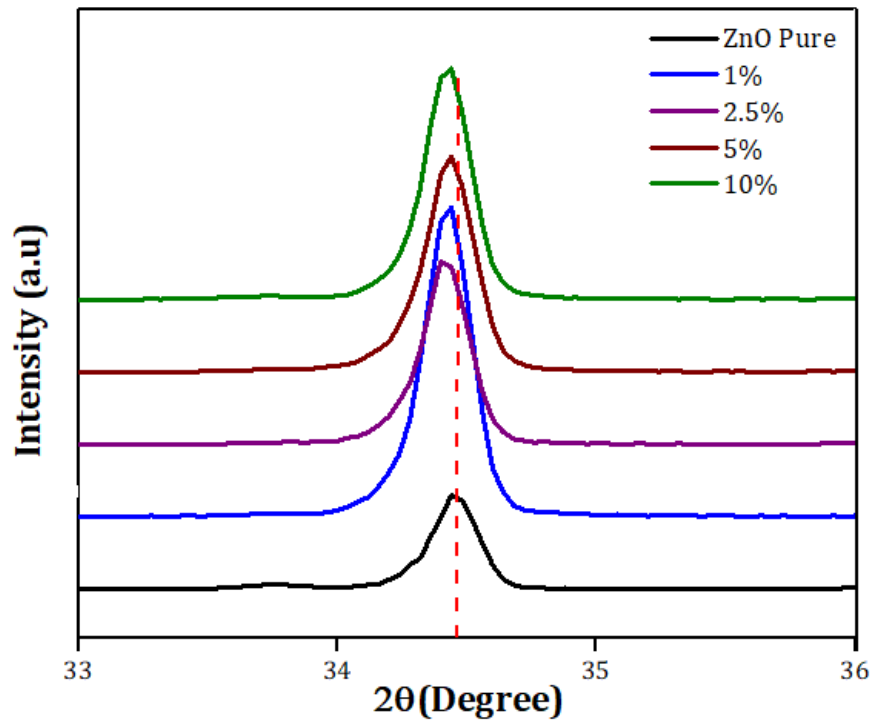


**Figure 2.** Position of (002) peak shifts of S-ZnO.

Calculated lattice parameters, FWHM and crystallite size of all samples are listed in Table 1. The lattice parameter calculation proceeds by means of the equation

$$\frac{1}{d_{hkl}^2} = \frac{4}{3}\frac{h^2+hk+k^2}{a^2} + \frac{l^2}{c^2} \qquad (2)$$

where $d_{hkl}$ is the distance between (h k l) planes, (h k l) are the Miller indices of the respective crystalline planes, a = b and c stand for the lattice parameters of the hexagonal ZnO structure. The crystalline phase of ZnO possesses lattice parameter of a and c of 3.253 Å and 5.204 Å respectively. As shown at Table 1, we have found that the parameter a decreases from 0.005 Å for 5 at.% but the parameter c slightly increases 0.005 Å for 2.5 at.% S doping ratio.

The average crystallite size (D) for the (002) plane of thin films was calculated using the Debye–Scherrer equation,

$$D = \frac{k\lambda}{\beta \cos \alpha} \qquad (3)$$

where, k, D and λ is, the Scherrer constant of 0.90, the average crystallite size and the wavelength of the X-ray ((0.15406 nm)), respectively. α is Bragg's angle, and β is the Full Width Half Maximum (FWHM) in radian. The FWHM value of X-ray diffraction peaks was obtained from the Gauss curve analysis. FWHM value is inversely proportional to crystal size. According to Table 1, the sample with the addition of sulfur has a larger crystallite size compared to the pure ZnO sample.

**Table 1** ZnO crystal lattice parameter data

| S doping ratio (at.%) | 2θ (°) | $D_{002}$ (Å) | a=b (Å) | c (Å) | FWHM (Degree) | Crystal Size (nm) |
|---|---|---|---|---|---|---|
| **0%** | 34.45 | 2.602 | 3.253 | 5.204 | 0.2282 | 36.3 |
| **1 %** | 34.42 | 2.603 | 3.252 | 5.206 | 0.2253 | 36.8 |
| **2.5 %** | 34.41 | 2.604 | 3.250 | 5.209 | 0.2263 | 36.7 |
| **5 %** | 34.43 | 2.603 | 3.248 | 5.206 | 0.2275 | 36.5 |
| **10 %** | 34.42 | 2.604 | 3.249 | 5.207 | 0.2218 | 37.4 |

According to FWHM as listed in Table 1, FWHM slightly decrease after the S addition. As the S concentration increases, the peak intensity and crystallite sizes become larger which imply the crystallinity improvement. This result is consistent with literature [17]. The highest crystallinity of S-doped ZnO has achieved at 10 at.% of S/ZnO film which has lowest FWHM and largest crystallite size..

**3.2 Surface Morphology and Elemental Composition**

Surface morphology and elemental composition of the samples were evaluated using FESEM and EDX. FESEM images and particle size distribution of ZnO and S-ZnO samples are shown in Figure 3. FESEM image with a scale of 200 nm displays the distribution of particles evenly growth on the FTO substrate. FESEM with a magnification of 50,000x (100nm scale) shows the geometric shape of the S-ZnO sample. Figure 3. (B) exhibits a pure ZnO nanorods with uniform shape of hexagonal (hexagonal) cross section. After doped with sulfur, the sample has a non-uniform nanorod shape due to the distortion of the cross-section shape changes with the size of each side is different which is clearly seen in Figure 3.3 (N). Distortion in the hexagonal side length of the nanorod gives a change in the value of the crystal lattice parameters. The addition of S atoms to ZnO shows spots on the ZnO cross-section surface that make the nanorod look rough which implies the formation of polycrystalline as well as the insertion of S atoms in the ZnO phase. This rough cross section of the nanorod was also obtained from research conducted by Sharma et al. [18]. The rough surface of the nanorod due to sulfidation can increase light scattering [16].

Figure 3. (N) shows the morphology of the 10% S sample which has the largest particle size and followed by the 5% S and 2.5% S samples shown in Figures 3 (H) and (K). Based on the calculation of standard deviations and the average particle size, the average diameter of S-ZnO nanorods ranges from 37.02 ± 7.046 nm to 69.22 ± 20.731 nm. These results indicate that the S- doped ZnO nanorod has uniform diameter distribution. The 1% S sample in Figure 3 (E) is the sample with the smallest particle size distribution even compared to the pure ZnO sample. Figure 3 (C), (F), (I), (L) and (O) show a histogram graph of the particle size distribution of each S-ZnO sample. The addition of S atoms to ZnO shows that the nanorod formed is compact compared to pure ZnO samples. So that the surface area is getting bigger because it covers the FTO substrate. Increasing the diameter size and density of the formed nanorod particles assume the growth rate of the nanorod due to sulfidation in the hydrothermal process. FESEM results with nanorod that are dense and grow perpendicular to the FTO substrate can increase the ability of light absorption.
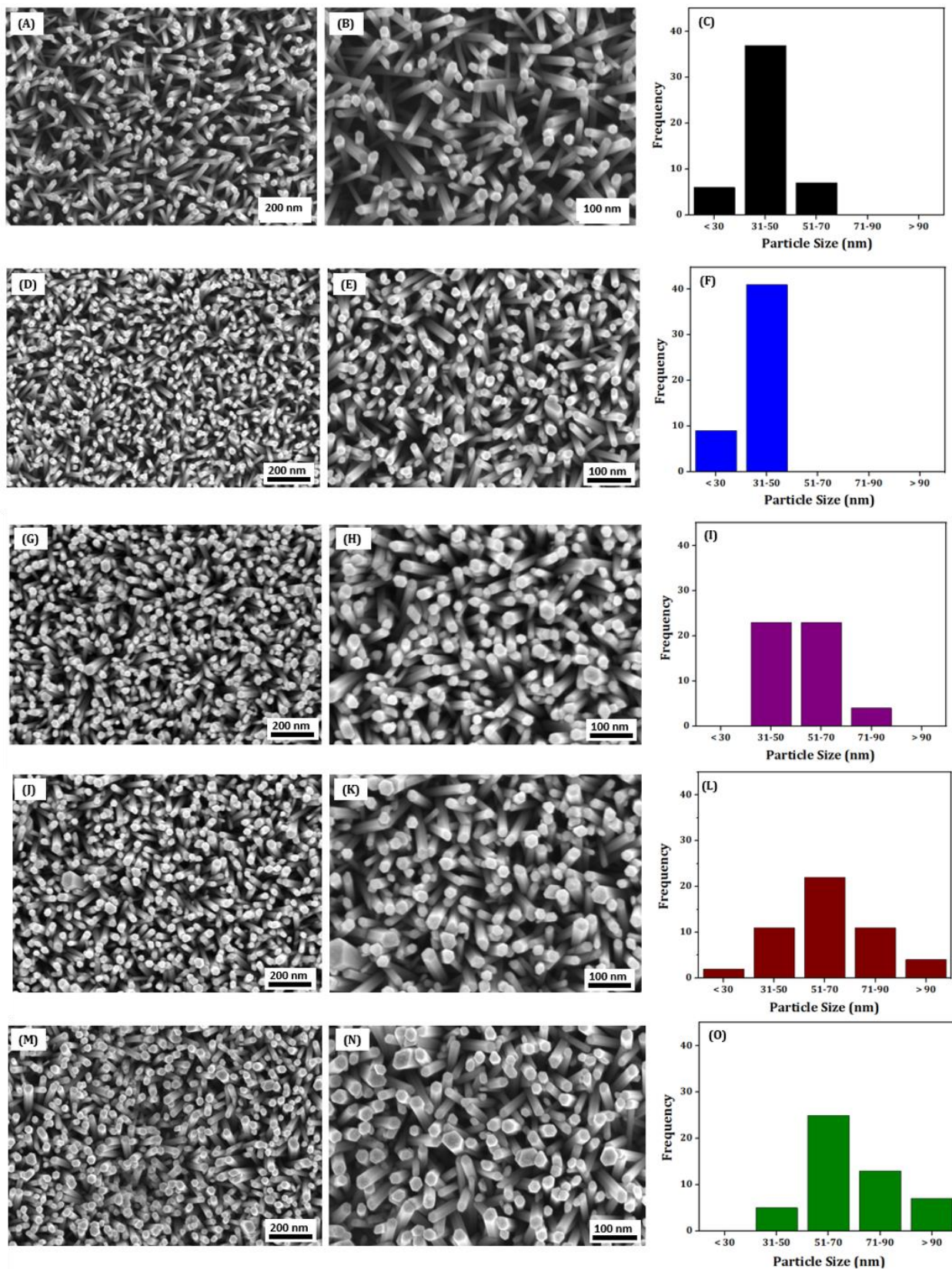
**Figure 3.** FESEM Images and particle size distribution of S-ZnO (A-C) ZnO Pure, (D-F) 1%S, (G-I) 2,5%S, (J-L) 5%S, and (M-O) 10%S.
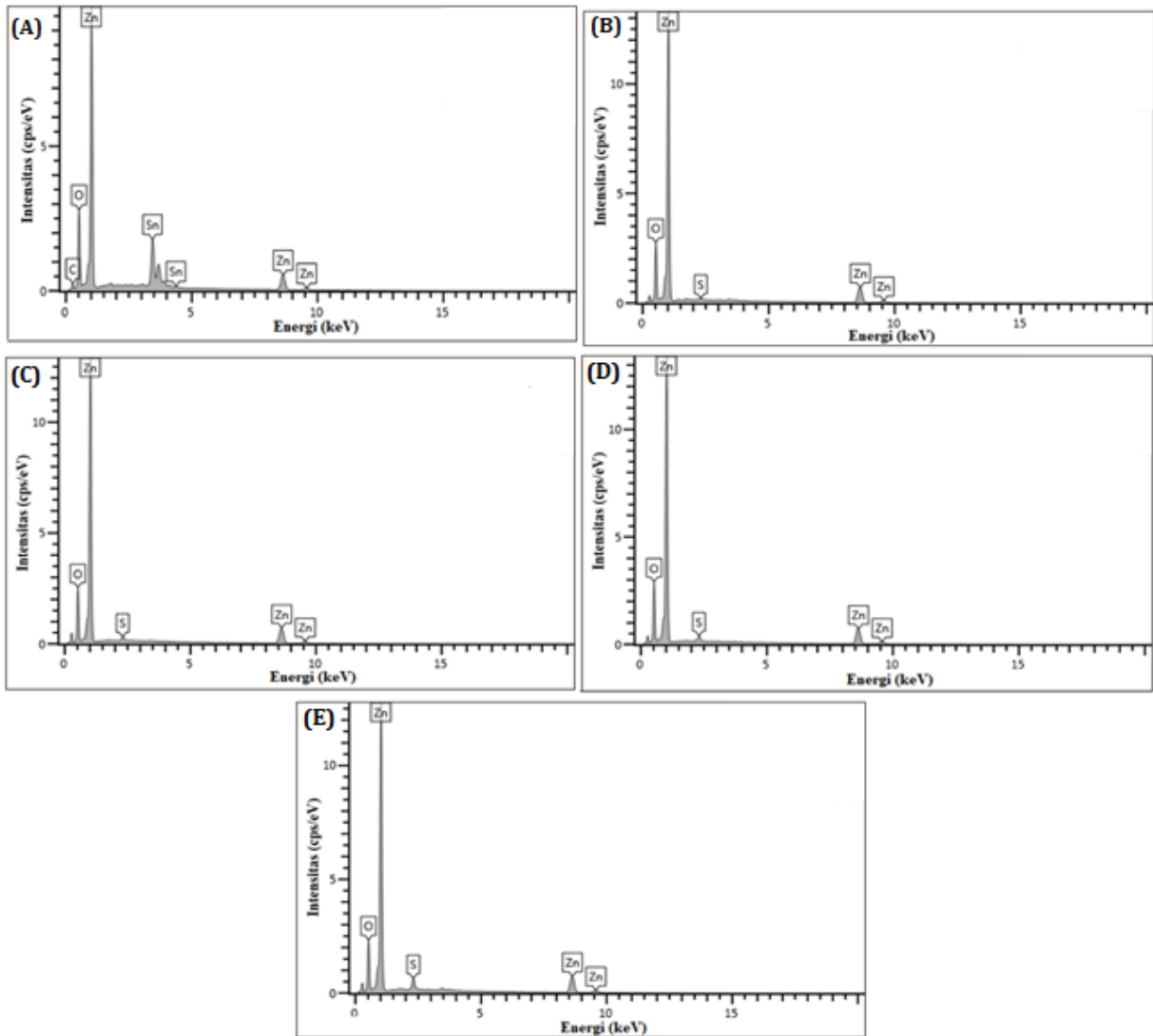
**Figure 4.** EDX Images of S-ZnO nanorod.

The distribution of elements from S-ZnO nanorod thin films can be seen from the results of the EDX spectrum shown in Figure 4 (A, B, C, D, and E is 0 at%, 1 at.%, 2.5 at.%, 5 at.% and 10 at.% S, respectively).The EDX spectrum results provide information about the composition and distribution of the elements contained by showing the percentage of weight of each element of the sample. Based on the results of this EDX spectrum, weight percentage of the given S element are proportional to the weight % of the S element obtained. The elements detected based on the EDX spectrum data results in Figure 4 include, Zinc (Zn), Oxygen (O), Sulfur (S), Tin (Sn) and Carbon (C) elements. Weight percentages of each constituent sample are presented in Table 2 below.

**Table 2** Weight percentages of S-ZnO

| Element | % Weight | | | | |
|---|---|---|---|---|---|
| | S-0 | S-1 | S-2,5 | S-5 | S-10 |
| Zn | 54,7 | 81,6 | 81,3 | 80,0 | 80,7 |
| O | 17,8 | 17,9 | 17,6 | 18,7 | 16,3 |
| S | - | 0,4 | 1,0 | 1,4 | 2,9 |
| Sn | 24,5 | - | - | - | - |
| C | 3,0 | - | - | - | - |
| Total | 100% | 100% | 100% | 100% | 100% |

The element that is not present in the pure ZnO sample is the sulfur element (S). The 10% S sample has the highest percentage of the S atomic that is equal to 2.9%, while the lowest percentage of the S atomic obtained in the sample 1% S is 0.4%. The percentage content of the S is higher with increasing S atom content in ZnO. In Figure 4 (A) which is a pure ZnO sample, there is the presence of Sn and C elements originating from the FTO substrate as a growth medium for ZnO material and from combustion during the sample annealing process, respectively.

### 3.3 Optical Properties

Figure 5 shows the optical absorbance of S-ZnO thin films. UV-Vis absorbance spectrum results show high optical absorption occurs in the wavelength range of 300-380 nm and low optical absorption in the visible light spectrum (380-800 nm). The optical absorption peak at the 378 nm wavelength is in accordance with the ZnO nanorod [19]. Based on the UV-Vis absorbance spectrum, the absorption rate of the S-ZnO sample increases with the percentage increase in the S to ZnO. The 5% sample sulfur has its own uniqueness, that is in the wavelength range of 340-370 nm there is a significant increase in absorbance compared to other samples. The maximum absorbance of pure ZnO and 1%S samples has the lowest absorbance of 1.80 a.u. While the highest absorption rate occurred in the 5% S sample of 2.10 a.u. Samples of 10 at.% and 2.5 at.% of S concentration have absorption values of 1.96 a.u and 1.92 a.u. However, in the visible light spectrum, the lowest to highest absorbance was found in pure ZnO samples, 1%, 2.5%, 5% and 10%. This increase in absorbance value is assumed to be due to the thickness of the sample which increases with the addition of S atoms. Where the more atoms produced, the more light absorbed will increase. It can also be thought to originate from the electron interaction between ZnO and S with an increase in S atomic (in the process of sulfidation) in ZnO[20].
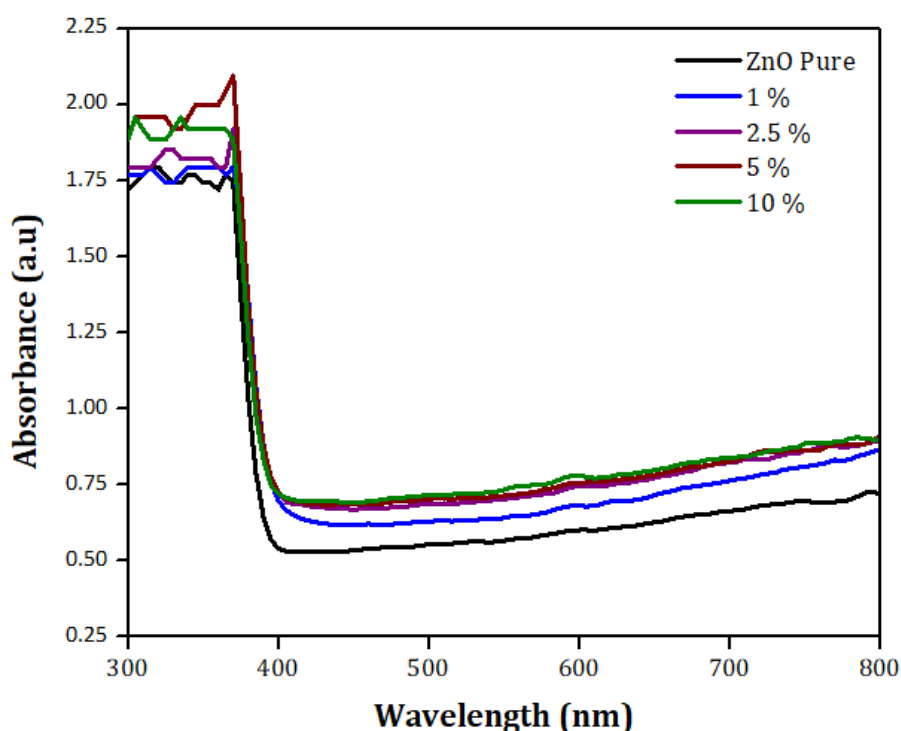


**Figure 5.** Absorbance spectra of S-ZnO sample with different dopant concentration.
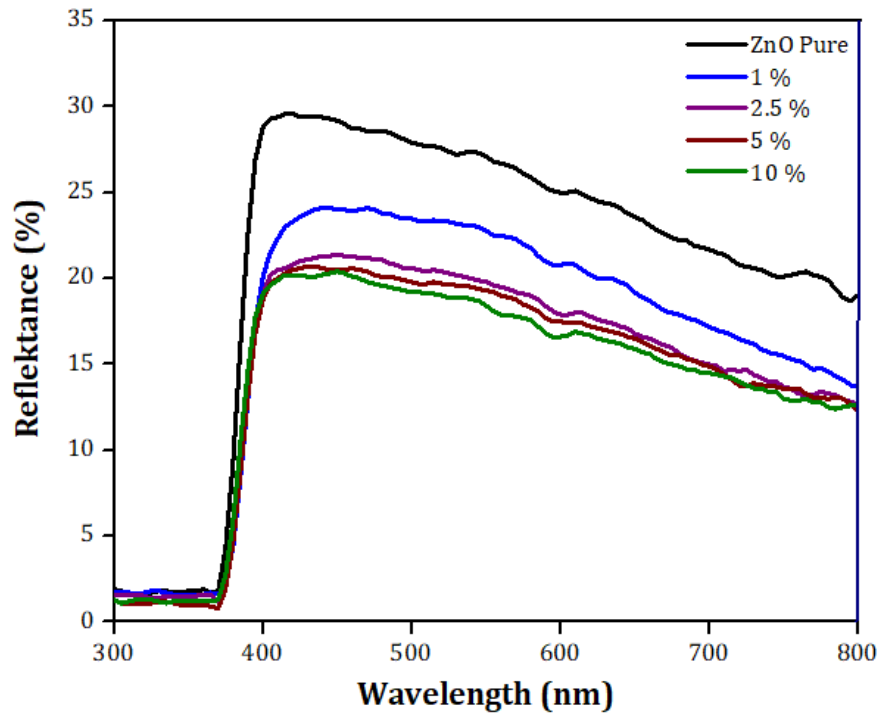
**Figure 6.** Diffuse reflectance spectra of S-ZnO thin films.

The optical reflectance of the S-ZnO samples were studied by analyzing the spectrum of UV-Vis diffuse reflectance in Figure 6. From this figure, it can be seen that the highest level of reflection occurs in the wavelength range of 380-800 nm in the visible light spectrum. While the low reflectance rate occurs in the UV-Vis spectrum (300-380 nm) which is the opposite of the absorbance spectrum curve. Based on the reflectance spectrum, the pure ZnO sample is the sample with the highest reflectance, which is 29.7% compared to the 1%, 2.5%, 5% and 10% sulfur samples respectively 24.2%, 21.5%, 20.7% and 20.5%. It can be seen that the sample with the addition of sulfur UV-Vis reflectance value has decreased and the peak reflectance of the sample shifts towards a greater wavelength.
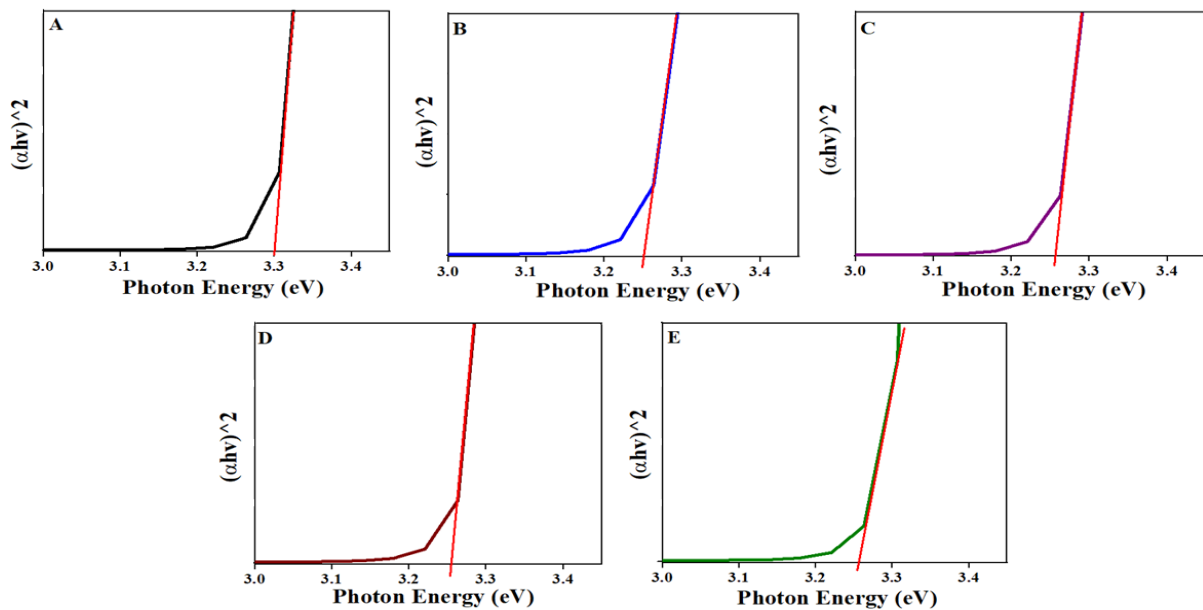


**Figure 7**. Tauc's plot for the determination of the band gap of the (a) ZnO pure (b) 1% S-ZnO (c) 2.5% S-ZnO (d) 5% S-ZnO and (e) 10 S-ZnO.

**Table 3** Optical Energy gap of S-ZnO

| Sample | Energy Gap (eV) |
|--------|-----------------|
| ZnO Pure | 3.30 |
| 1% | 3.25 |
| 2.5% | 3.26 |
| 5 % | 3.25 |
| 10 % | 3.26 |

The energy gap of a material can be calculated from the extrapolation results of the $h\upsilon$ vs $(\alpha h\upsilon)^2$ curve which is the result of transformation of the UV-Vis reflectance spectrum. Figure 7 is the Tauc plot curve of $h\upsilon$ vs $(\alpha h\upsilon)^2$ nanorod S-ZnO samples with various atomic ratio S to ZnO. The amount of energy gap is obtained from the intersection of a straight line on the curve with respect to $h\upsilon$ on the X-axis. Table 3 shows the magnitude of the energy gap of the S-ZnO nanorod sample with various the atomic ratio S to Zn. Based on Table 3 the amount of energy gap obtained is in the range of 3.25-3.30 eV. The acquisition of this gap energy value is smaller with the addition of sulfur [21]. Samples with the lowest energy gap are 1% S-ZnO and 5% S-ZnO with energy gap of 3.25 eV.

The S-ZnO thin film photoluminescence spectrum is shown in Figure 8. S-ZnO samples (0-10 at% S) show the peak emission occurring at a wavelength of 406 nm for all samples. These emission bands represent violet emissions caused by electron transitions from the interstitial Zn level to the valence band [22]. The highest emission intensity obtained is owned by the sample with the highest doping of 10 at.% S. Emission intensity is related to the crystal quality of the S-ZnO sample.
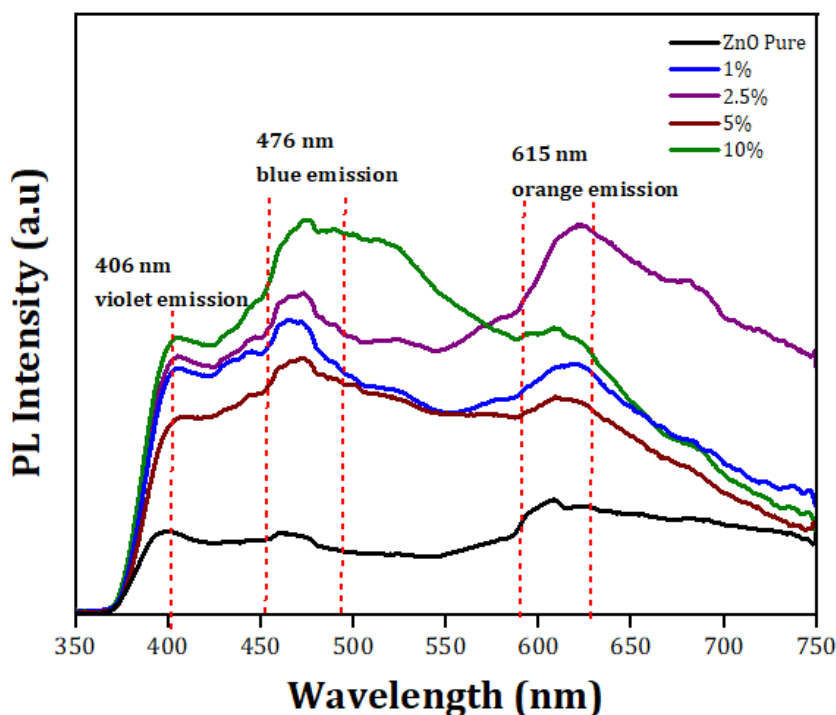


**Figure 8.** Photoluminescence spectra of S-ZnO.

The ZnO nanorod sample has a visible light emission band known as Deep Level Emissions (DLE). The peak emission of S-ZnO samples at wavelengths of 476 nm and 615 nm corresponds to the blue emission band and orange emission band. High emission peaks in the visible light spectrum of ZnO nanorods indicate more structural defects and decrease the crystal quality [23].

## 4. CONCLUSION

Pure ZnO and S-doped ZnO thin films have been synthesized using seed-mediated hydrothermal method. XRD analysis reveals that sulfur-doped ZnO at 10 at.% has improve the crystallinity of ZnO thin films. FESEM analysis shows that the morphology of ZnO thin-film have hexagonal nanorod shape and uniform size distribution. UV-Vis spectroscopy revealed that ZnO and S-ZnO thin films possess the optical band gap energy in the range of 3.23 eV. Based on its optical and structural properties, S-ZnO thin films fabricated by seed mediated hydrothermal method have the potential as an alternative material for solar cell applications and photocatalyst application.

## REFERENCES

[1] D. D. O. Eya, A. J. Ekpunobi, C. E. Okeke, "Structural and optical properties and applications of zinc oxide thin films prepared by chemical bath deposition technique," Pacific J. Sci. Technol. **6**, 1 (2005) 16–22.

[2] H. Morkoc, U. Ozgur, "Zinc oxide: fundamentals, materials and device technology," in Processing, Devices, and Heterostructures, Federal Republic of German: WILEY-VCH Verlag GmbH & Co. KGaA, Weinheim, (2009) 446–454.

[3] G. G. Rusu, P. Gorley, C. Baban, A. P. Rambu, M. Rusu, "Preparation and characterization of Mn-doped ZnO thin films," J. Optoelectron. Adv. Mater. **12**, 4 (2010) 895–899.

[4] F. A. Garcés, N. Budini, R. R. Koropecki, R. D. Arce, "Structural analysis of ZnO(: Al,Mg) thin films by X-ray diffraction," Procedia Mater. Sci. **8**, November (2015) 551–560.

[5] O. Bayram, E. Sener, E. İgman, O. Simsek, "Investigation of structural, morphological and optical properties of nickel-doped zinc oxide thin films fabricated by co-sputtering," J. Mater. Sci. Mater. Electron. **30**, 4 (2019) 3452–3458.

[6] G. Poongodi, P. Anandan, R. M. Kumar, R. Jayavel, "Studies on visible light photocatalytic and antibacterial activities of nanostructured cobalt doped ZnO thin films prepared by sol-gel spin coating method," Spectrochim. Acta - Part A Mol. Biomol. Spectrosc, (2015).

[7] R. Jothi Ramalingam, A. K. Shukla, K. Kombaiah, J. J. Vijaya, A. M. Tawfeek, "Synthesis, characterization and optical properties of sulfur and fluorine doped ZnO nanostructures for visible light utilized catalysis," Optik (Stuttg). **148** (2017) 325–331.

[8] A. Khan, M. I. Ahmed, A. Adam, A. M. Azad, M. Qamar, "A novel fabrication methodology for sulfur-doped ZnO nanorods as an active photoanode for improved water oxidation in visible-light regime," Nanotechnology **28**, 5 (2017).

[9] X. Y. Xie *et al.,* "Synthesis of S-doped ZnO by the interaction of sulfur with zinc salt in PEG200," J. Alloys Compd. **644** (2015) 383–389.

[10] P. C. Kuo, S. Y. Chen & J. S. Bow, "Development and photoluminescence of ZnO-ZnS core-shell nanotube and nanorod arrays," Key Eng. Mater. **351** (2007) 70–74.

[11] Z. Wang, S. W. Cao, S. C. J. Loo, C. Xue, "Nanoparticle heterojunctions in ZnS-ZnO hybrid nanowires for visible-light-driven photocatalytic hydrogen generation," CrystEngComm. **15**, 28 (2013) 5688–5693.

[12] F. Fabbri *et al.,* "S-induced modifications of the optoelectronic properties of ZnO mesoporous nanobelts," Sci. Rep. **6**, June (2016) 1–8.

[13] I. Hussain, H. P. Tran, J. Jaksik, J. Moore, N. Islam, and M. J. Uddin, "Functional materials, device architecture, and flexibility of perovskite solar cell," Emergent Mater.**1**, 3–4 (2018) 133–154.

[14] S. H. Deulkar, J. L. Huang, M. Neumann-Spallart, "Zinc oxysulfide thin films grown by pulsed laser deposition," J. Electron. Mater. **39**, 5 (2010) 589–594.

[15] C. Justin Raj, S. N. Karthick, K. V. Hemalatha, M. K. Son, H. J. Kim, K. Prabakar, "Magnesium doped ZnO nanoparticles embedded ZnO nanorod hybrid electrodes for dye sensitized solar cells," J. Sol-Gel Sci. Technol. **62**, 3 (2012) 453–459.

[16] L. Wei & Y. Chen, "PDXScholar High-Performance Self-Powered Photodetectors Based on ZnO / ZnS Core-Shell Nanorod Arrays Follow this and additional works at: http://pdxscholar.library.pdx.edu/mengin_fac," [2016].

[17] T. Özdal, R. Taktakoğlu, H. Özdamar, M. Esen, D. K. Takçı, H. Kavak, "Crystallinity improvement of ZnO nanorods by optimization of low-cost electrodeposition technique Teoman," Thin Solid Films **592** (2015) 143–149.

[18] A. Sharma, P. Sahoo, R. Thangavel, "A study on photoelectrochemical properties of ZnO@ZnS nanostructures synthesized via facile ion-exchange approach," AIP Conf. Proc. **1961** (2018).

[19] A. A. Umar, S. K. Md Saad, M. I. Ali Umar, M. Y. A. Rahman, M. Oyama, "Advances in porous and high-energy (001)-faceted anatase $TiO_2$ nanostructures," Opt. Mater. (Amst). **75** (2018) 390–430.

[20] Y. C. Liang, C. C. Wang, "Surface crystal feature-dependent photoactivity of ZnO-ZnS composite rods: Via hydrothermal sulfidation," RSC Adv. **8**, 9 (2018) 5063–5070.

[21] P. V. Raleaooa, A. Roodt, G. G. Mhlongo, D. E. Motaung, R. E. Kroon, O. M. Ntwaeaborwa, "Luminescent, magnetic and optical properties of ZnO-ZnS nanocomposites," Phys. B Condens. Matter **507**, November (2017) 13–20.

[22] A. A. M. Farag, M. Cavas, F. Yakuphanoglu, F. M. Amanullah, "Photoluminescence and optical properties of nanostructure Ni doped ZnO thin films prepared by sol-gel spin coating technique," J. Alloys Compd. **509**, 30 (2011) 7900–7908.

[23] S. Iwan, V. Fauzia, A. A. Umar, X. W. Sun, "Room temperature photoluminescence properties of ZnO nanorods grown by hydrothermal reaction," AIP Conf. Proc. **1729** (2016) 1–5.